The Neuronal Voltage-Dependent Sodium Channel Type II IQ Motif Lowers the Calcium Affinity of the C-Domain of Calmodulin†

Nathaniel T. Theoharis, Brenda R. Sorensen, Jesse Theisen-Toupal,‡ and Madeline A. Shea*

Department of Biochemistry, Roy J. and Lucille A. Carver College of Medicine, University of Iowa, Iowa City, Iowa 52242−1109

Received July 3, 2007; Revised Manuscript Received October 10, 2007

ABSTRACT: Calmodulin (CaM) is the primary calcium sensor in eukaryotes. Calcium binds cooperatively to pairs of EF-hand motifs in each domain (N and C). This allows CaM to regulate cellular processes via calcium-dependent interactions with a variety of proteins, including ion channels. One neuronal target is $Na_V1.2$, voltage-dependent sodium channel type II, to which CaM binds via an IQ motif within the $Na_V1.2$ C-terminal tail (residues 1901−1938) [Mori, M., et al. (2000) *Biochemistry 39*, 1316−1323]. Here we report on the use of circular dichroism, fluorescein emission, and fluorescence anisotropy to study the interaction between CaM and $Na_V1.2$ at varying calcium concentrations. At 1 mM $MgCl_2$, both full-length CaM (CaM_{1-148}) and a C-domain fragment (CaM_{76-148}) exhibit tight (nanomolar) calcium-independent binding to the $Na_V1.2$ IQ motif, whereas an N-domain fragment of CaM (CaM_{1-80}) binds weakly, regardless of calcium concentration. Equilibrium calcium titrations of CaM at several concentrations of the $Na_V1.2$ IQ peptide showed that the peptide reduced the calcium affinity of the CaM C-domain sites (III and IV) without affecting the N-domain sites (I and II) significantly. This leads us to propose that the CaM C-domain mediates constitutive binding to the $Na_V1.2$ peptide, but that interaction then distorts calcium-binding sites III and IV, thereby reducing their affinity for calcium. This contrasts with the CaM-binding domains of voltage-dependent Ca^{2+} channels, kinases, and phosphatases, which increase the calcium binding affinity of the C-domain of CaM.

Calmodulin (CaM) is an essential eukaryotic protein that consists of 148 amino acids (∼17 kDa) and has two sequentially and structurally homologous domains: the N-domain (CaM_{1-80},[1] which encompasses calcium-binding sites I and II) and the C-domain (CaM_{76-148}, which encompasses calcium-binding sites III and IV). Each CaM domain contains two EF-hand, helix−loop−helix, calcium-binding motifs. Between the domains is a flexible linker region, comprised of residues 76−80 (see Figure 1A), which not only tethers the two domains but also lowers the calcium binding affinity and increases the thermal stability of the N-domain (*1*, *2*). The two calcium-binding sites in each domain bind calcium cooperatively, with calcium-binding sites III and IV having a higher affinity than sites I and II (*3*−*6*). CaM is important in numerous cell signaling pathways (*7*−*12*) and is involved in regulation of metabolic enzymes, cyclases, esterases, phosphatases, kinases, cytoskeletal molecules, and ion channels (*13*).

As more CaM targets have been identified, it has been suggested that CaM functions in regulation of ion channel gating (*7*). CaM has been shown to interact with the C-terminal tail of several ion channels, including those of the NMDA (*14*−*16*), SK (*17*), L-type Ca^{2+} (*18*, *19*), and P/Q Ca^{2+} (*20*) families. Nagayama and colleagues first demonstrated such an interaction in the type II isoform ($Na_V1.2$) of the rat neuronal voltage-dependent sodium channel (VDSC) (*21*). This particular VDSC isoform is necessary for the propagation of an action potential along unmyelinated axons (*22*, *23*).

The VDSC is comprised of one α-subunit (260 kDa) and one or more *β*-subunits (33−36 kDa each) (*24*). The α-subunit of the channel is the pore-forming entity and is comprised of four homologous domains (I−IV). Sodium channel inactivation occurs via an interaction involving the intracellular loop between domains III and IV (*12*, *25*) and the C-terminal tail (*26*−*29*) of the α-subunit that results in channel closure. The proximal half of this tail has been modeled to contain six α-helices (*28*), and deletion of the putative sixth α-helix region slows recovery from inactivation, maintaining the channel in a closed, inactivated state (*26*, *28*, *29*). A classic CaM-binding IQ motif [(I,L,V)-QXXXRXXXX(R,K), where X is any amino acid (Figure 1B)] lies between residues 1901 and 1927 within the proposed sixth α-helix region of the $Na_V1.2$ isoform of the

† Supported by a grant to M.A.S. from the National Institutes of Health (RO1 GM 57001).

* To whom correspondence should be addressed. Telephone: (319) 335-7885. Fax: (319) 335-9570. E-mail: madeline-shea@uiowa.edu.

‡ Current address: Pritzker School of Medicine, University of Chicago, Chicago, IL 60637-5415.

[1] Abbreviations: apo, calcium-depleted; CaM_{1-148}, full-length mammalian calmodulin, residues 1−148; CaM_{1-80}, N-domain fragment of calmodulin, residues 1−80; CaM_{76-148}, C-domain fragment of calmodulin, residues 76−148; CD, circular dichroism; EGTA, ethylene glycol bis(aminoethyl ether)-*N*,*N*,*N*′,*N*′-tetraacetic acid; F-$Na_V1.2$ IQp, fluorescein-labeled peptide corresponding to residues 1901−1927 from $Na_V1.2$; F-STOP, splice variant of stable tubule-only polypeptide; HEPES, *N*-(2-hydroxyethyl)piperazine-*N*′-2-ethanesulfonic acid; $Na_V1.2$, neuronal voltage-dependent sodium channel type II; $Na_V1.2$ IQp, peptide corresponding to residues 1901−1927 from $Na_V1.2$; NTA, nitrilotriacetic acid; Oregon Green, Oregon Green 488 BAPTA-5N.

10.1021/bi7013129 CCC: $40.75
Published on Web 12/08/2007

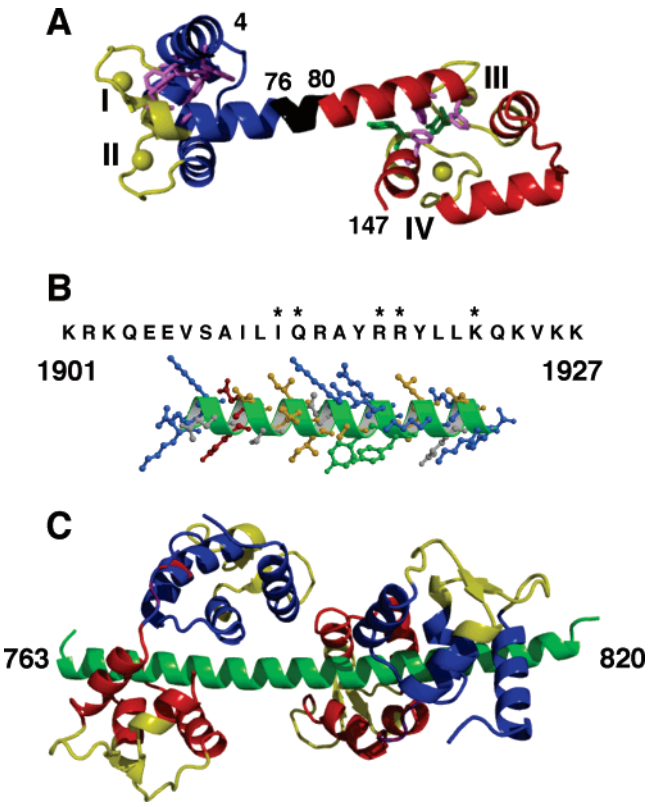

FIGURE 1: Structures of CaM and a helical model of $Na_V1.2$ IQp. (A) Ribbon drawing of a 1.7 Å crystal structure of $(Ca^{2+})_4$-CaM (PDB entry 1cll) (*66*). The N-domain (blue), C-domain (red), and flexible linker region shared by both domains (residues 76−80) (black) are shown. Aromatic residues are represented as sticks, and tyrosine (green) and phenylalanine (violet) are indicated. Calcium and its binding sites are labeled I−IV (yellow). (B) Sequence and helical model representation of $Na_V1.2$ IQp (residues 1901−1927). Asterisks above the sequence highlight residues that define the IQ motif. Basic residues (blue), acidic residues (red), tyrosines Y1916 and Y1919 (green), hydrophobic residues (yellow), and polar/uncharged residues (gray) in the model are indicated. (C) Ribbon drawing of apo CaM (N-domain, blue; C-domain, red) in complex with a peptide (green, residues 763−820) containing the first two IQ motifs of the murine myosin V heavy chain (PDB entry 2IX7) (*42*). Calcium-binding sites are colored yellow. All figures were created using Sybyl 6.5 (MIPS3-IRIX 6.2, Tripos Associated Inc.) and MacPymol 0.98.

ion channel (*21*). Targets containing this motif primarily associate with CaM in a calcium-independent fashion (*30*). A ClustalW alignment of the IQ-containing CaM binding region of $Na_V1.2$ identified a high degree of sequence identity to corresponding regions of all 10 known human VDSC isoforms (*31*, *32*). A helical representation of the IQ motif from rat $Na_V1.2$ is shown in Figure 1B.

Recent studies of VDSC isoforms $Na_V1.4$, $Na_V1.5$, and $Na_V1.6$ have shown that CaM binding is necessary for the generation of functional sodium currents, suggesting that CaM plays a regulatory role with regard to these channels (*29*, *33*, *34*). It is possible that the N- and C-domains of CaM have distinct regulatory roles in sodium channel modulation, as they do for other channels. The first physiological evidence of differential roles for the two domains of CaM came from in vivo studies reported by Kung and associates (*35*). These investigators performed a genetic screen of mutagenized *Paramecium* and identified two classes of viable mutants: those that under- or over-reacted to chemical stimuli. These mutants were found to be defective in the regulation of their calcium-dependent sodium and potassium channel currents, and the responsible mutations were mapped to the CaM-encoding gene. Under-reacting mutations, which localized between sites I and II or in site II of the CaM N-domain, were shown to affect only sodium conductance. In contrast, over-reacting mutations were found to localize within sites III and IV and in the fourth helix of the C-domain and affected only potassium conductance. Subsequently, the two CaM domains have been shown to have distinct roles in regulating other ion channels, including the ryanodine receptor (*36*), the NMDA receptor (*16*), and the L-type calcium channel (*37*, *38*). Apo (calcium-depleted) CaM can associate (via the C-domain) with these targets prior to calcium influx.

Atomic-resolution structures of CaM bound to peptides derived from several target proteins have shown that CaM can interact with targets at various degrees of calcium saturation. For example, calcium-saturated CaM [$(Ca^{2+})_4$-CaM] is bound to a small peptide from skeletal myosin light chain kinase (PDB entry 2BBM) (*39*); on the other hand, $(Ca^{2+})_2$-CaM (sites III and IV occupied) binds to a large fragment of the anthrax edema factor (PDB entry 1K90) (*40*), and $(Ca^{2+})_2$-CaM (sites I and II occupied) binds to a fragment of the SK channel (PDB entry 1G4Y) (*41*). A recent high-resolution structure of 2 equiv of apo CaM bound to a peptide containing the first two IQ motifs in the myosin V heavy chain (Figure 1C; PDB entry 2IX7) illustrates that one CaM interacts with each IQ motif, with each CaM C-domain in a semi-open conformation and each CaM N-domain in a closed conformation (*42*). Therefore, it is clear that complete calcium occupancy of CaM is not required for target association. The effect of calcium binding on this association, however, is not clear and is likely target-specific.

The mechanism by which CaM associates and activates the VDSC is not known. Studies of the $Na_V1.5$ isoform indicate that apo CaM binds to the $Na_V1.5$ IQ motif via its C-domain, and both CaM domains bind in the presence of calcium, albeit with weaker affinity (*43*). This model of domain-specific association is consistent with those proposed for interactions of CaM with other ion channels (*36*). The structures of apo CaM bound to the IQ motifs of myosin V (*42*) support this model and suggest that the interaction of an IQ motif with the C-domain would be energetically more favorable than that with the N-domain. Studies of interaction of CaM with C-terminal fragments of $Na_V1.2$ (residues 1777−1937) and $Na_V1.5$ (residues 1773−1940) illustrate a calcium-independent association that is required for proper folding of these termini and show that association decreases the affinity of the C-domain of CaM for calcium (*44*). It is not clear whether each domain of CaM has a separable role in this interaction or what effect this interaction has on the calcium affinity of the N-domain of CaM. In this study, we compared the binding affinity of full-length CaM (CaM_{1-148}) and fragments of the domains, as represented by CaM_{1-80} and CaM_{76-148}, for a peptide derived from the $Na_V1.2$ IQ motif region (residues 1901−1927, $Na_V1.2$ IQp), under both calcium-depleted and calcium-saturating conditions. The results show that the C-domain of CaM binds with very high affinity ($\leq$10 nM) in a calcium-independent manner, and the interaction with the N-domain is orders of magnitude weaker.

Our conclusions, which are based on circular dichroism (CD), fluorescence emission spectra, and anisotropy analyses,

lead us to suggest that CaM preassociates with the IQ peptide from this ion channel (i.e., is bound at low intracellular Ca^{2+} concentrations) via its C-domain. Equilibrium calcium titrations show that the calcium affinity of sites III and IV in the C-domain decreases significantly upon addition of $Na_V1.2$ IQp, while the calcium affinity of sites I and II in the N-domain increases slightly, resulting in an overall decrease in the calcium affinity of the molecule. This is in contrast to most earlier studies of the calcium binding affinity of CaM bound to a peptide, which have shown that the addition of the peptide leads to an increase in calcium affinity (*7*, *36*, *45*−*50*). Our data represent the first direct demonstration that this IQ motif leads to a selective decrease in the calcium affinity of the C-domain to an extent such that the N-domain has a slightly higher affinity than the C-domain.

MATERIALS AND METHODS

Overexpression and Purification of Calmodulin. Reagents were of the highest grade commercially available. Full-length mammalian calmodulin (CaM_{1-148}) and both the N-domain (CaM_{1-80}) and C-domain (CaM_{76-148}) fragments were cloned and overexpressed using standard methods (*51*). The proteins were purified as described by Putkey (*52*), with a subsequent 10 min incubation at 80 °C in the presence of a saturating level of calcium (10 mM $CaCl_2$) to precipitate any remaining contaminating proteins. The recombinant proteins were 97−99% pure as judged by silver-stained SDS−PAGE or reversed-phase HPLC. Protein concentrations were determined from UV absorbance in 0.1 N NaOH, and the phenylalanine and tyrosine content was estimated using the extinction coefficients reported by Beaven and Holiday (*53*).

Peptides. The $Na_V1.2$ IQ peptide ($Na_V1.2$ IQp) corresponds to residues 1901−1927 of the α-subunit of rat $Na_V1.2$ (acetyl-Lys-Arg-Lys-Gln-Glu-Glu-Val-Ser-Ala-Ile-Val-Ile-Gln-Arg-Ala-Tyr-Arg-Arg-Tyr-Leu-Leu-Lys-Gln-Lys-Val-Lys-Lys-coNH_2) and has a molecular mass of 3402.15 Da as measured using MALDI-TOF (University of Iowa College of Medicine Molecular Analysis Facility). Addition of 5,6-carboxyfluorescein label to the amino terminus of the peptide (resulting in F-$Na_V1.2$ IQp) increased the molecular mass to 3720.01 Da (MALDI-TOF). Both were synthesized at the W. M. Keck Biotechnology Resource Center (Yale University, New Haven, CT) and found to be 99% pure by HPLC analysis.

Circular Dichroism (CD). Spectra were recorded using an Aviv 62DS instrument with a 1 cm path length quartz cuvette (QS 1.000), and scanning from 260 to 215 nm in 0.5 nm increments; five scans were averaged for each sample, and a minimum of three independent replicates were conducted. Spectra for apo CaM_{1-148}, CaM_{1-80}, and CaM_{76-148} (5 μM) with and without $Na_V1.2$ IQp (7 μM) were recorded in 2 mM HEPES, 100 mM KCl, 5 mM NTA, 0.05 mM EGTA, and 1 mM $MgCl_2$ (pH 7.4) at 22 °C. To ensure calcium depletion, EGTA was added to each sample to a final concentration of 200 μM. Calcium saturating conditions were achieved by adding concentrated $CaCl_2$ in the same buffer to a final concentration of 10 mM. Figure 2 shows (a) representative experimental spectra of $Na_V1.2$ IQp, CaM_{1-148}, CaM_{1-80}, and CaM_{76-148} alone, (b) spectra of solutions of CaM and $Na_V1.2$ IQp, and (c) simulations of the sum of average spectra of $Na_V1.2$ IQp alone (7 μM) and

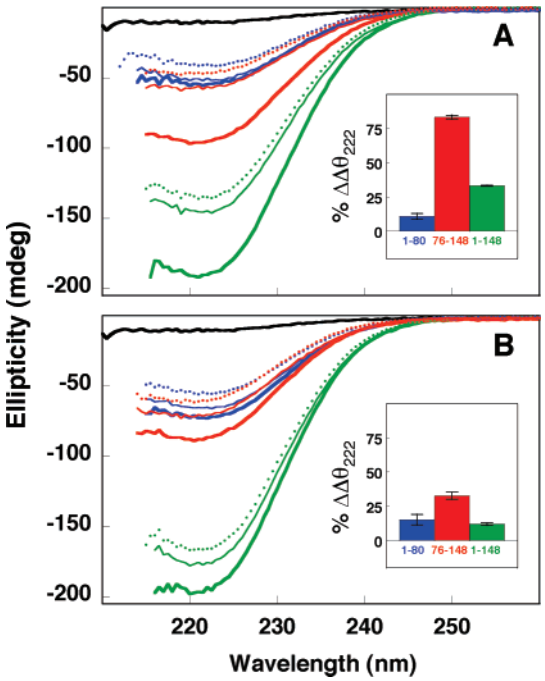

FIGURE 2: Effect of $Na_V1.2$ IQp on circular dichroism spectra of CaM. Observed spectra of apo (A) or calcium-saturated (B) CaM (5 μM) [CaM_{1-80} (blue), CaM_{76-148} (red), and CaM_{1-148} (green)] alone (dotted curves) and in the presence of $Na_V1.2$ IQp (7 μM; thick solid curves). Simulated spectra (thin solid curves) represent the sum of the spectra of CaM alone (dotted curves) and $Na_V1.2$ IQp (7 μM, solid black curve). The buffer consisted of 2 mM HEPES, 100 mM KCl, 5 mM NTA, 0.05 mM EGTA, and 1 mM $MgCl_2$ (pH 7.4) at 22 °C with or without 10 mM $CaCl_2$. Insets show the percent increase in negative ellipticity at 222 nm of the CaM with $Na_V1.2$ IQp sample beyond that expected for noninteracting solutes, calculated as $\Delta\theta_{222}^{Obs} - \Delta\theta_{222}^{Sim}$ (eq 1). Bar graph colors correspond to forms of CaM shown in panels A and B.

CaM alone (5 μM), to indicate the expected result for noninteracting solutes.

The ellipticity of CaM alone (Figure 2, dotted curves) was used as a reference state to compare the ellipticity of solutions of (i) $Na_V1.2$ IQp and apo CaM (Figure 2A, thick solid curves) and (ii) $Na_V1.2$ IQp and calcium-saturated CaM (Figure 2B, thick solid curves) and (iii) simulated spectra (Figure 2, thin solid curves) obtained by adding those of CaM alone to that of the peptide alone according to eq 1

$$\Delta\theta_{222} = \frac{\theta_{222} - \theta_{250}}{\theta_{222}^{CaM} - \theta_{250}^{CaM}} \quad (1)$$

where θ_{222} (representative of the most negative signal) and θ_{250} (representative of the baseline "zero" signal) are the ellipticities at 222 and 250 nm, respectively, and θ_{222}^{CaM} and θ_{250}^{CaM} are the observed ellipticities of CaM alone at 222 and 250 nm, respectively. The value used for θ_{222} or θ_{222}^{CaM} was obtained by averaging five readings between 221 and 223 nm to minimize the contribution of instrument noise. The fractional change in ellipticity in excess of that attributed to individual solutes ($\Delta\Delta\theta_{222}$ in Figure 2 insets) was calculated as the difference in $\Delta\theta_{222}$ for the observed spectra and the $\Delta\theta_{222}$ for the simulated spectra ($\Delta\theta_{222}^{Obs} - \Delta\theta_{222}^{Sim}$).

Fluorescein Emission Spectra of F-$Na_V1.2$ IQp. Emission spectra of fluorescein in F-$Na_V1.2$ IQp (1 μM) with or without 3 μM CaM_{1-148}, CaM_{1-80}, or CaM_{76-148} were

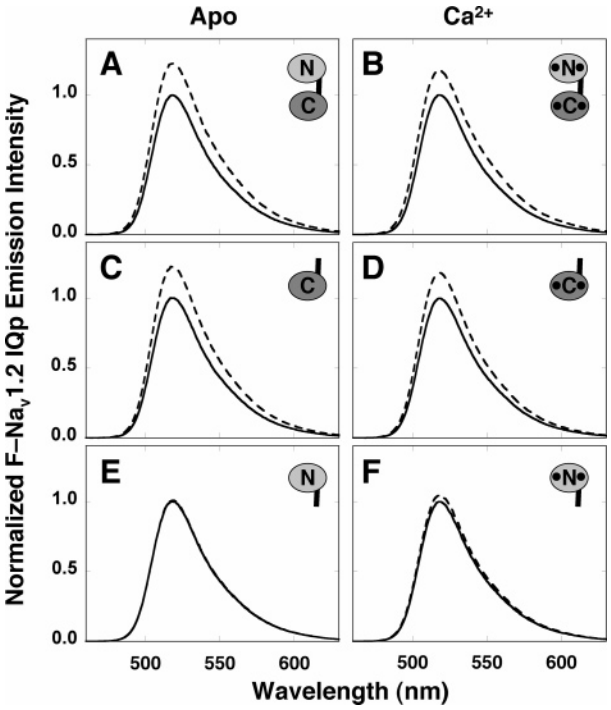

FIGURE 3: Change in fluorescein emission spectra of F-$Na_V1.2$ IQp upon addition of CaM. Normalized emission spectra of 1 μM apo (dashed lines, left panels) and calcium-saturating (dashed lines, right panels) F-$Na_V1.2$ IQp alone (solid lines) and after the addition of 3 μM CaM_{1-148} (A and B), CaM_{1-80} (C and D), or CaM_{76-148} (E and F) in 50 mM HEPES, 100 mM KCl, 5 mM NTA, 0.05 mM EGTA, and 1 mM $MgCl_2$ (pH 7.4) at 22 °C with or without 10 mM $CaCl_2$ (λ_{ex} = 430 nm).

collected with a Fluorolog 3 fluorimeter (Jobin Yvon, Edison, NJ) at 0.5 nm increments using a λ_{ex} of 430 nm, slit widths (equivalent to bandpasses) of 2 nm (excitation) and 10 nm (emission), and a temperature of 22 °C. Apo samples in 50 mM HEPES, 100 mM KCl, 5 mM NTA, 0.05 mM EGTA, and 1 mM $MgCl_2$ (pH 7.4) at 22 °C were saturated with calcium by the addition of $CaCl_2$ in matching buffer to a final concentration of 10 mM. Each spectrum was normalized $[(F_x - F_{min})/(F_{max} - F_{min})]$ to the λ_{max} (518 nm) of F-$Na_V1.2$ IQp alone, was corrected for dilution, but was not corrected for the wavelength response characteristics of the instrument. Representative spectra are shown in Figure 3.

Fluorescence Anisotropy. The fluorescence anisotropy of F-$Na_V1.2$ IQp (1 μM) was monitored upon addition of apo or calcium-saturated CaM (10 μM to 1 mM stocks) using a Fluorolog3 fluorimeter (Jobin Yvon) with a λ_{ex} of 430 nm, a λ_{em} of 518 nm, slit widths of 2 nm (excitation) and 10 nm (emission), and a temperature of 22 °C. Apo buffer contained 50 mM HEPES, 100 mM KCl, 5 mM NTA, 0.05 mM EGTA, and 1 mM $MgCl_2$ (pH 7.4). Calcium saturating buffer contained all components of the apo buffer and 10 mM $CaCl_2$. Anisotropy (R) was calculated using eq 2

$$R = \frac{I_{VV} - GI_{VH}}{I_{VV} + 2GI_{VH}} \quad (2)$$

where I_{VV} is the intensity of vertically excited and vertically emitted light and I_{VH} is the intensity of vertically excited and horizontally emitted light. G equals I_{HV}/I_{HH}, with I_{HV} being the intensity of horizontally excited and vertically emitted light and I_{HH} the intensity of horizontally excited and horizontally emitted light (*54*). Each anisotropy reading resulted from monitoring the sample for 2 s and averaging at least three readings.

Table 1: Equilibrium Binding Constants of CaM Binding to F-$Na_V1.2$ IQp

	apo[a]		calcium-saturated[a]	
protein	K_d	ΔG_{assn}[b]	K_d	ΔG_{assn}[b]
CaM_{1-148}	≤10 nM	≤−10.8	≤10 nM	≤−10.8
CaM_{1-80}	132 ± 3 μM	−5.24 ± 0.02	5.40 ± 2.96 μM	−7.18 ± 0.35
CaM_{76-148}	≤25 nM	≤−10.27	≤75 nM	≤−9.62

[a] The buffer contained 50 mM HEPES, 100 mM KCl, 5 mM NTA, 0.05 mM EGTA, and 1 mM $MgCl_2$ with or without 10 mM $CaCl_2$ (pH 7.4). [b] $\Delta G_{assn} = -RT \ln(1/K_d)$, reported in kilocalories per mole (1 kcal = 4.184 kJ).

Each curve was normalized to the R_{max} of F-$Na_V1.2$ IQp $[(R_x - R_{min})/(R_{max} - R_{min})]$ and plotted against the total CaM concentration ($[CaM_{total}]$). The F-$Na_V1.2$ IQp−CaM complex exhibited a 1:1 stoichiometry. To estimate the affinity of CaM for F-$Na_V1.2$ IQp, normalized data were fit to a one-site Langmuir binding isotherm described by eq 3 using NONLIN (*55*)

$$\overline{Y_1} = \frac{K_a[CaM_{free}]}{1 + K_a[CaM_{free}]} \quad (3)$$

where K_a represents the association constant (the reciprocal of the dissociation constant, K_d) and $[CaM_{free}]$ equals the concentration of unbound CaM, calculated from the two independent variables, $[CaM_{total}]$ and the total concentration of $Na_V1.2$ ($[F\text{-}Na_V1.2\ IQp_{total}]$), according to the quadratic equation (eq 4)

$$[CaM_{free}] = \frac{-b \pm \sqrt{b^2 - 4K_a(-[CaM_{total}])}}{2K_a} \quad (4)$$

where $b = 1 + K_a[F\text{-}Na_V1.2\ IQp_{total}] - K_a[CaM_{total}]$. The affinity for apo and calcium-saturated CaM_{1-80} was weak, and $[CaM_{free}] \cong [CaM_{total}]$. However, the affinity for apo and calcium-saturated CaM_{1-148} and CaM_{76-148} was high enough that $[F\text{-}Na_V1.2\ IQp_{total}] \geq 10K_d$. While this condition is appropriate for determining the stoichiometry of binding, it is not appropriate for resolving accurate affinities of binding because $[CaM_{free}]$ is limiting (*56*, *57*). To obtain limiting values for the affinity under those conditions, $[CaM_{free}]$ was estimated iteratively in the nonlinear least-squares analysis as the difference between $[CaM_{total}]$ and $[CaM_{bound}]$ (calculated as $[F\text{-}Na_V1.2\ IQp_{total}]\overline{Y_1}$) (see Table 1). To account for dilution of $[Na_V1.2_{total}]$, this concentration was included as a second independent variable in the analysis.

Equation 5 accounted for experimental variations in the observed end point signals of individual titration curves:

$$f(X) = Y_{[X]low} + \bar{Y}_1(Y_{[X]high} - Y_{[X]low} = span) \quad (5)$$

where $Y_{[X]low}$ corresponds to the fluorescence anisotropy of F-$Na_V1.2$ IQp alone (no added CaM), $\bar{Y}_1$ refers to the average fractional saturation of F-$Na_V1.2$ IQp (eq 3), and $Y_{[X]high} - Y_{[X]low}$ or span accounts for the magnitude and direction (i.e., positive for an increasing signal and negative for a decreasing

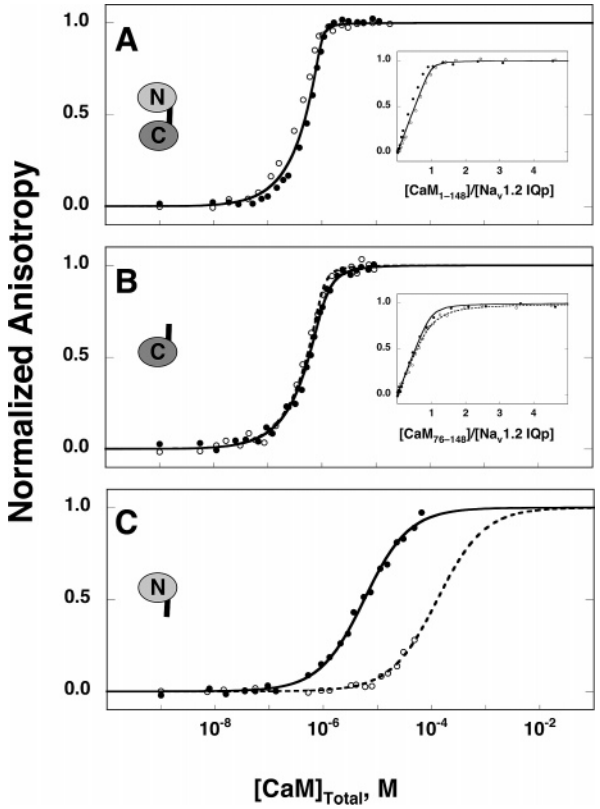

FIGURE 4: Change in the fluorescence anisotropy of F-Na_V1.2 IQp upon titration with CaM. The normalized anisotropy of 1 μM F-Na_V1.2 IQp (λ_{ex} = 430 nm, λ_{em} = 518 nm) increased upon titration with apo (open) and calcium-saturated (closed) CaM_{1-148} (A), CaM_{76-148} (B), or CaM_{1-80} (C) in 50 mM HEPES, 100 mM KCl, 0.05 mM EGTA, 5 mM NTA, and 1 mM $MgCl_2$ with or without 10 mM $CaCl_2$ (pH 7.4) at 22 °C. The absolute anisotropy increased from 0.05 to 0.09 (CaM_{1-148}), 0.07 (CaM_{76-148}), and 0.08 (CaM_{1-80}). Curves through the data were simulated to a one-site binding isotherm (eq 3), fixing [F-Na_V1.2 IQp_{total}] to 1 μM. Data were renormalized to the fitted values for $Y_{X[low]}$ and span. The data for the titration with apo CaM_{1-80} [panel C (○)] were normalized to a maximum anisotropy equal to that obtained upon subsequent titration of the apo CaM_{1-80}/F-Na_V1.2IQp sample with concentrated solutions of $CaCl_2$. These normalized data were fit to eq 5 with *span* fixed at 1. Insets illustrate the change in normalized anisotropy with increasing [CaM_{1-148}]/[Na_V1.2 IQp] (A) or [CaM_{76-148}]/[Na_V1.2 IQp] (B), where [Na_V1.2 IQp] was 1 μM.

signal) of steady-state fluorescence upon binding. Data shown in Figure 4 were renormalized to the fitted $Y_{X[low]}$ and span. Curves through the data were simulated using eq 5 and a fixed [F-Na_V1.2 IQp_{total}] equal to the initial concentration of 1 μM.

In titrations of F-Na_V1.2IQp with apo CaM_{1-80}, the fluorescence anisotropy of F-Na_V1.2IQp did not reach a plateau at the final [CaM_{total}] tested (65 μM CaM_{1-80}). To determine the affinity of F-Na_V1.2 IQp for apo CaM_{1-80}, the data were normalized to a maximum anisotropy equal to that obtained upon subsequent titration of the apo CaM_{1-80}/F-Na_V1.2 IQp sample with a concentrated solution of $CaCl_2$. These normalized data were fit to eq 5, and the span was fixed to 1.

Equilibrium Calcium Titrations. Equilibrium calcium titrations were monitored at 22 °C using an SLM 4800C fluorimeter (SLM Instruments Inc., Urbana, IL) with slit widths set at 8 nm. CaM alone (CaM_{1-148}, CaM_{1-80}, or CaM_{76-148} at 3 μM) or with Na_V1.2 IQp at two different concentrations [4.2 μM (molar ratio of 1:1.4) and 8.4 μM (molar ratio of 1:2.8)] in 50 mM HEPES, 100 mM KCl, 5 mM NTA, 0.05 mM EGTA, 1 mM $MgCl_2$, and 0.1 μM Oregon Green (pH 7.4) was titrated using a concentrated calcium solution (25 mM to 1 M $CaCl_2$ in the same buffer). For this purpose, a microburet (Micro-Metric Instrument Co., Cleveland, OH) was fitted with a 250 μL Hamilton syringe (Hamilton Co., Reno, NV). Binding of calcium to the N-domain (sites I and II) was monitored by the intrinsic phenylalanine fluorescence (λ_{ex} = 250 nm, λ_{em} = 280 nm), and binding to the C-domain (sites III and IV) was monitored by the intrinsic tyrosine fluorescence (λ_{ex} = 277 nm, λ_{em} = 320 nm) as previously described (*58*). Calcium did not change the tyrosine fluorescence of Na_V1.2 IQp (*31*), and calcium binding to sites III and IV of CaM was proportional to the change in tyrosine signal as monitored during stoichiometric calcium titrations (*31*). The fluorescent calcium indicator dye Oregon Green 488 BAPTA-5N (OregonGreen, 0.1 μM) (Molecular Probes, Eugene, OR) was used to determine the free calcium concentration at each point in the titration (see eq 6) (for discussion, see ref *59*).

$$[\text{calcium}]_{\text{free}} = K_d \frac{f_{\text{high}} - f_{[X]}}{f_{[X]} - f_{\text{low}}} \quad (6)$$

In this equation, f_{high} and f_{low} are the highest and lowest observed fluorescence intensity signals, respectively, observed for Oregon Green during the titration. The K_d of calcium binding to Oregon Green was determined to be 34.24 μM in 50 mM HEPES, 100 mM KCl, and 1 mM $MgCl_2$ (pH 7.4) at 22 °C (λ_{ex} = 494 nm, λ_{em} = 521 nm) (*2*). Calcium titrations of CaM samples at three molar ratios of Na_V1.2 IQp (0, 1.4, and 2.8) were repeated at least three times; Figures 5 and 6 each show representative titrations.

Free Energies of Calcium Binding. Each CaM domain may be considered to be a two-site macromolecule as described by the linkage diagram below.

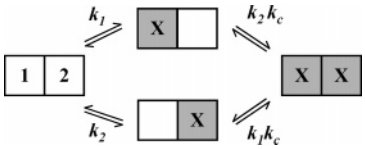

Free energies of calcium binding to sites I and II or sites III and IV were determined by fitting the titration data to a model-independent two-site (Adair) function (eq 7) as described previously (*51*, *58*, *60*).

$$\bar{Y} = \frac{K_1[X]^1 + 2K_2[X]^2}{2(1 + K_1[X]^1 + K_2[X]^2)} \quad (7)$$

In this equation, the macroscopic association constant K_1 is the sum of intrinsic microscopic equilibrium constants (k_1 + k_2) for two sites: either sites I and II in the N-domain or sites III and IV in the C-domain. This formulation allows the microscopic binding constants (k_1 and k_2) to be nonequivalent. The second macroscopic equilibrium constant K_2 is the product of the intrinsic microscopic equilibrium constants and the cooperativity constant ($k_1k_2k_c$). The parameters ΔG_1 and ΔG_2 are macroscopic binding free energies, with ΔG_i being equal to $-RT \ln K_i$. The parameter ΔG_2

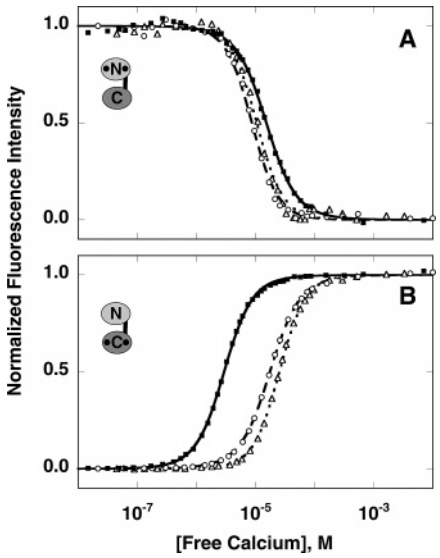

FIGURE 5: Equilibrium calcium titrations of CaM_{1-148} at several molar ratios of $Na_V1.2$ IQp, monitored using intrinsic CaM fluorescence. (A) Phenylalanine fluorescence (λ_{ex} and λ_{em} of 250 and 280 nm, respectively) and (B) tyrosine fluorescence (λ_{ex} and λ_{em} of 277 and 320 nm, respectively): CaM alone (■), 1:1.4 CaM:$Na_V1.2$ IQp (○), and 1:2.8 CaM:$Na_V1.2$ IQp (△). Fitted free energies of CaM alone (solid lines), 1:1.4 CaM:$Na_V1.2$ IQp (dashed lines), and 1:2.8 CaM:$Na_V1.2$ IQp (dotted lines) were simulated using values in Table 2 and eq 8. Calcium titrations were performed with 3 μM CaM and/or 4.2 or 8.4 μM $Na_V1.2$ IQp in 50 mM HEPES, 100 mM KCl, 5 mM NTA, 0.05 mM EGTA, 1 mM $MgCl_2$, and 0.1 μM Oregon Green (pH 7.4) at 22 °C.

is thus the total free energy of saturating both calcium-binding sites in a domain, while ΔG_1 corresponds to the free energy of saturating a single calcium-binding site in a domain.

Changes in fluorescence intensity for the calcium titrations were normalized to the highest and lowest experimentally determined signals. To account for finite variations in the asymptotes of replicate titrations, the function [f(X)] used for nonlinear least-squares analysis is given by eq 8

$$f(\mathrm{X}) = Y_{[\mathrm{X}]\mathrm{low}} + \bar{Y} \times span \tag{8}$$

where $\bar{Y}$ refers to the average fractional saturation as described by eq 7 and $Y_{[X]low}$ corresponds to the value of fluorescence intensity at the lowest calcium concentration of the titration being fit. The parameter *span* was negative in the case of a decreasing signal (phenylalanine, sites I and II) and positive in the case of an increasing signal (tyrosine, sites III and IV). Values for all parameters were fit simultaneously using NONLIN (*55*).

NONLIN provides several measures of the goodness of fit for the parameters that minimize the variance of each fit. These error statistics include (a) the value of the square root of variance, (b) the values of asymmetric 65% confidence intervals, (c) the systematic trends in the distribution of residuals, (d) the magnitude of the span of residuals, and (e) the absolute value of elements of the correlation matrix. From these, best-fit values were selected after trying several sets of initial guesses for parameters to probe for the presence of local minima. When analyzing titration curves based on changes in the phenylalanine signal, we could not independently resolve the value of ΔG_1 (calcium binding to site I or II) in all cases, and these ΔG_1 values were fixed at values yielding a consistently low square root of variance. This constituted a manual grid search approach to determining the lowest square root of variance.

The average total free energies (ΔG_2) resolved for calcium binding to the N-domain (sites I and II) and C-domain (sites III and IV) are reported in Table 2 for at least three experiments under each condition. The changes in the total free energy of calcium binding to CaM induced by $Na_V1.2$ IQp ($\Delta\Delta G_2$) are reported in Table 2. One representative titration of CaM_{1-148} is presented in Figure 5, and one representative titration of CaM_{1-80} and CaM_{76-148} is presented in Figure 6.

Fractional Populations of Ligation Species. In Figure 8, the fractional populations of liganded species were calculated using the standard equation for the Boltzmann distribution. The probability (f_s) of a single species (s) of a macromolecule is given by eq 9

$$f_s = \frac{\exp(-\Delta G_s/RT)[\mathrm{X}]^j}{\sum_{s,j} \exp(-\Delta G_s/RT)[\mathrm{X}]^j} \tag{9}$$

where [X] is the ligand activity, ΔG_s represents the Gibbs free energy [$-RT \ln(K_s)$] of species s, and j represents the stoichiometry of ligand(s) binding to species s. Each free energy (ΔG_s) is the sum of the intrinsic and cooperative interactions that apply to that species. The denominator of this expression is Z, the binding polynomial for the macromolecule.

A general partition function describing the 16 possible species of CaM requires four intrinsic equilibrium constants (k_I, k_{II}, k_{III}, and k_{IV}) for calcium binding to each of the EF-hand sites, and at least two intradomain cooperativity terms (k_{I-II} and k_{III-IV}). Specifically, Z is $1 + (k_I + k_{II} + k_{III} + k_{IV})[\mathrm{X}] + (k_Ik_{II}k_{I-II} + k_Ik_{III} + k_Ik_{IV} + k_{II}k_{III} + k_{II}k_{IV} + k_{III}k_{IV}k_{III-IV})[\mathrm{X}]^2 + (k_Ik_{II}k_{III}k_{I-II} + k_{III}k_{IV}k_{III-IV}k_I + k_{III}k_{IV}k_{III-IV}k_{II} + k_Ik_{II}k_{I-II}k_{IV})[\mathrm{X}]^3 + k_Ik_{II}k_{III}k_{IV}k_{I-II}k_{III-IV}[\mathrm{X}]^4$. The individual states are represented by a linear array of four digits according to the pattern of vacancy (0) or occupancy (1) of each of the four sites (e.g., apo CaM is represented as [0000], whereas CaM with sites III and IV occupied is [0011]).

Curves shown in Figure 8 were simulated using eq 9 assuming $k_I = k_{II}$, $k_{III} = k_{IV}$, and ΔG_1 values resolved from fits of the CaM_{1-80} and CaM_{76-148} data to eq 8. In the absence of $Na_V1.2$ IQp, these values were as follows: $k_I = k_{II} = 1.362 \times 10^4\ M^{-1}$, $k_{III} = k_{IV} = 4.272 \times 10^4\ M^{-1}$, and cooperativity terms k_{I-II} and k_{III-IV} of 78.8 and 208.5 M^{-1}, respectively. In the presence of $Na_V1.2$ IQp, these values were as follows: $k_I = k_{II} = 1.730 \times 10^4\ M^{-1}$, $k_{III} = k_{IV} = 2.837 \times 10^4\ M^{-1}$, $k_{I-II} = -95.1\ M^{-1}$, and $k_{III-IV} = 12.5\ M^{-1}$.

RESULTS

The major aim of this study was to determine the domain-specific properties of CaM binding to the $Na_V1.2$ IQp and how these change upon calcium binding. To this end, multiple spectroscopic techniques, including circular dichroism, fluorescence spectra, fluorescence anisotropy, and fluorescence-monitored calcium titrations, were used.

Circular Dichroism. The binding of $Na_V1.2$ IQp to CaM was explored by monitoring peptide-induced changes in

Table 2: Effect of $Na_V1.2$ IQp on the Apparent Total Free Energy of Calcium Binding to CaM

		sites I and II (Phe)		sites III and IV (Tyr)	
protein	CaM:IQp ratio	ΔG_2[a]	$\Delta\Delta G_2$[b]	ΔG_2[a]	$\Delta\Delta G_2$[b]
CaM_{1-148}	1:0	-13.01 ± 0.09	–	-14.95 ± 0.14	–
CaM_{1-148}	1:1.4	-13.76 ± 0.16	-0.75 ± 0.18	-12.89 ± 0.07	2.06 ± 0.16
CaM_{1-148}	1:2.8	-13.64 ± 0.35	-0.63 ± 0.36	-12.58 ± 0.28	2.37 ± 0.31
CaM_{1-80}	1:0	-12.91 ± 0.09	–		
CaM_{1-80}	1:1.4	-13.30 ± 0.03	-0.39 ± 0.09		
CaM_{1-80}	1:2.8	-13.40 ± 0.33	-0.49 ± 0.34		
CaM_{76-148}	1:0			-14.81 ± 0.10	–
CaM_{76-148}	1:1.4			-12.69 ± 0.08	2.12 ± 0.13
CaM_{76-148}	1:2.8			-12.61 ± 0.13	2.20 ± 0.16

[a] Gibbs free energies reported in kilocalories per mole (1 kcal = 4.184 kJ). Free energies and errors represent averages and standard deviations for at least three trials. [b] $\Delta\Delta G_2$ is the difference between the ΔG_2 of the CaM−$Na_V1.2$ IQp complex and the ΔG_2 of CaM (alone) reported in kilocalories per mole [$\Delta\Delta G_2 = \Delta G_2$(CaM−$Na_V1.2$ IQp) − ΔG_2(CaM)]. Errors are propagated.

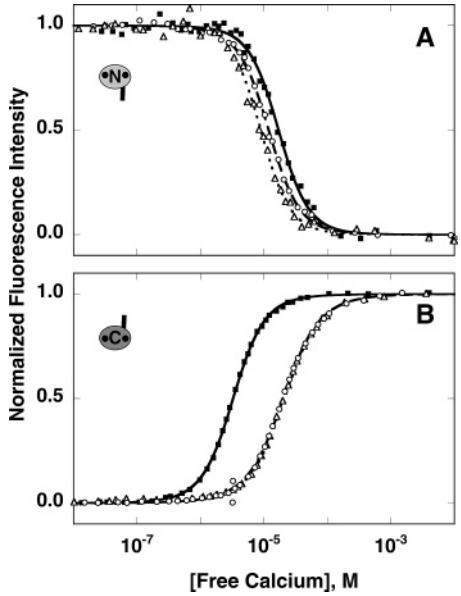

FIGURE 6: Equilibrium calcium titrations of CaM domain fragments at several molar ratios with $Na_V1.2$ IQp, monitored using intrinsic CaM fluorescence. (A) CaM_{1-80} − phenylalanine fluorescence (λ_{ex} and λ_{em} of 250 and 280 nm, respectively) and (B) CaM_{76-148} − tyrosine fluorescence (λ_{ex} and λ_{em} of 277 and 320 nm, respectively): CaM alone (■), 1:1.4 CaM:$Na_V1.2$ IQp (○), and 1:2.8 CaM:$Na_V1.2$ IQp (△). Fitted free energies of CaM alone (solid lines), 1:1.4 CaM:$Na_V1.2$ IQp (dashed lines), and 1:2.8 CaM:$Na_V1.2$ IQp (dotted lines) were simulated using values from Table 2 and eq 8. Calcium titrations were performed with 3 μM CaM and/or 4.2 or 8.4 μM $Na_V1.2$ IQp in 50 mM HEPES, 100 mM KCl, 5 mM NTA, 0.05 mM EGTA, 1 mM $MgCl_2$, and 0.1 μM Oregon Green (pH 7.4) at 22 °C.

ellipticity in the far-UV region, which reflects changes in overall secondary structure. The ellipticity of $Na_V1.2$ IQp alone was near zero (black curve) in apo (Figure 2A) or calcium-saturating (Figure 2B) buffer (see Materials and Methods), reflecting minimal ordered secondary structure in the absence of CaM. As reported previously (*61*), both apo (Figure 2A) and calcium-saturated CaM_{1-148} (Figure 2B) had a large negative ellipticity at 222 nm (dotted green line), consistent with its high degree of α-helical content observed in atomic-resolution structures (Figure 1). The spectra of apo and calcium-saturated CaM_{1-80} (Figure 2, dotted blue) and CaM_{76-148} (Figure 2, dotted red) also exhibited a minimum in ellipticity at 222 nm. For each protein sample, a simulated spectrum (thin solid curve) was calculated as the sum of a spectrum for CaM alone and one for $Na_V1.2$ IQp alone.

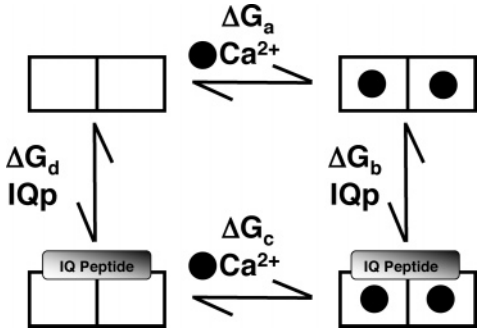

FIGURE 7: Linkage diagram of calcium and $Na_V1.2$ IQp binding to one domain of CaM. Each box represents one calcium-binding site within CaM. Filled circles represent calcium; IQ peptide (oblong box) represents $Na_V1.2$ IQp. Conservation of energy requires that $\Delta G_a + \Delta G_b = \Delta G_c + \Delta G_d$.

These represent the expected CD spectra for noninteracting components (i.e., no association between CaM and $Na_V1.2$ IQp).

Consistent with previous studies (*62*), the addition of $Na_V1.2$ IQp increased the negative ellipticity of the solution beyond what would be expected for noninteracting solutes (i.e., $\Delta\Delta\theta_{222}$ was positive). The largest increases were observed for apo CaM_{76-148} [83.4 ± 1.4% (Figure 2A inset)] and apo CaM_{1-148} [33.3 ± 0.3% (Figure 2A inset)]. For calcium-saturated forms of these proteins, the peptide-induced changes ($\Delta\Delta\theta_{222}$) were smaller: 32.7 ± 2.6% for calcium-saturated CaM_{76-148} and 12.0 ± 0.9% for calcium-saturated CaM_{1-148} (Figure 2B inset). Thus, the observed change exceeded that predicted for independent solutes (shown by thin solid curves), providing evidence for association. The greater change in ellipticity of apo CaM samples likely reflects the fact that apo CaM is less thermostable and more flexible than calcium-saturated CaM (*51*, *63*); therefore, association of peptide with CaM causes a greater net change in the ellipticity of an apo CaM sample.

In contrast with CaM containing the C-domain, the peptide-induced change ($\Delta\Delta\theta_{222}$) in apo CaM_{1-80} was only 10.9 ± 2.1% (Figure 2A) while that of calcium-saturated CaM_{1-80} was 15.2 ± 3.9% (Figure 2B). These changes were small and did not provide convincing evidence of association between the N-domain of CaM and $Na_V1.2$ IQp at the concentrations that were tested.

F-$Na_V1.2$ IQp Fluorescein Emission Spectra in the Presence of CaM. Domain-specific binding of CaM to $Na_V1.2$ IQp was explored by monitoring the change in emission of

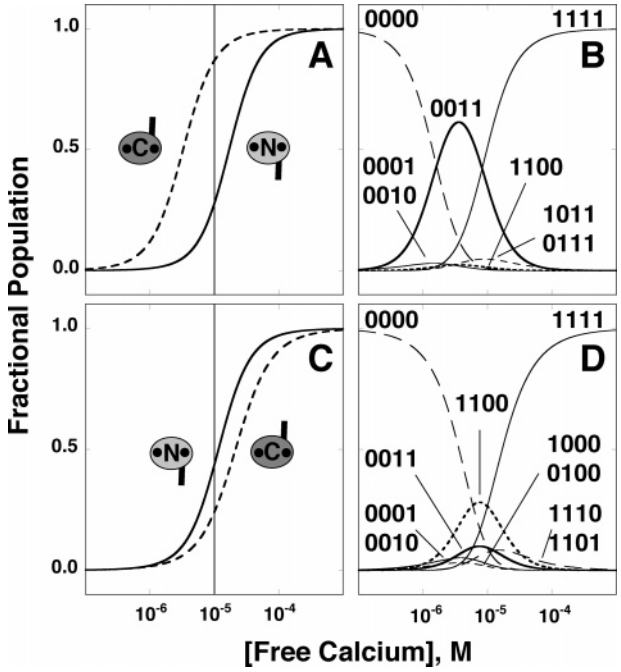

FIGURE 8: Calcium-dependent fractional populations of CaM domains in the presence or absence of $Na_V1.2$ IQp. Fractional populations of CaM_{1-80} (solid lines) and CaM_{76-148} (dashed lines) alone (A) and in the presence of $Na_V1.2$ IQp (C) were simulated using eq 7. The ligation species with population abundances that were >0.02 are shown for CaM alone (B) or in the presence of $Na_V1.2$ IQp (D). These were simulated using eq 9 assuming $k_I = k_{II}$, $k_{III} = k_{IV}$, and ΔG_1 values resolved from fits of the CaM_{1-80} and CaM_{76-148} data to eq 8. In the absence of $Na_V1.2$ IQp, these values were as follows: $k_I = k_{II} = 1.362 \times 10^4\ M^{-1}$; $k_{III} = k_{IV} = 4.272 \times 10^4\ M^{-1}$; cooperativity terms k_{I-II} and k_{III-IV} were 78.8 and 208.5 M^{-1}, respectively. In the presence of $Na_V1.2$ IQp, these values were as follows: $k_I = k_{II} = 1.730 \times 10^4\ M^{-1}$; $k_{III} = k_{IV} = 2.837 \times 10^4\ M^{-1}$; $k_{I-II} = -95.1\ M^{-1}$ and $k_{III-IV} = 12.5\ M^{-1}$. The occupancies of the four sites in the order I, II, III, and IV for curves shown are indicated as empty (0) or filled (1).

fluorescein-labeled apo or calcium-saturated $Na_V1.2$ IQp (F-$Na_V1.2$ IQp) upon addition of CaM_{1-148}, CaM_{1-80}, or CaM_{76-148} (Figure 3). The addition of either CaM_{1-148} or CaM_{76-148} increased the fluorescein emission of apo F-$Na_V1.2$ IQp by ~23% (that of CaM_{1-148} by 22.8 ± 0.3% and that of CaM_{76-148} by 22.7 ± 0.2%) and calcium-saturated F-$Na_V1.2$ IQp by ~20% (that of CaM_{1-148} by 18.5 ± 3.0% and that of CaM_{76-148} by 21.9 ± 2.9%). In contrast, the interaction of CaM_{1-80} with F-$Na_V1.2$ IQp was calcium-dependent; the fluorescein emission of apo F-$Na_V1.2$ IQp (0.6 ± 1.1%) was not changed by the addition of CaM_{1-80}, whereas the fluorescein emission of calcium-saturated F-$Na_V1.2$ IQp was increased slightly (by 5.1 ± 2.3%) in the presence of CaM_{1-80}.

F-$Na_V1.2$ IQp Fluorescence Anisotropy in the Presence of CaM. The fluorescence anisotropy of F-$Na_V1.2$ IQp was used to establish the stoichiometry of the F-$Na_V1.2$ IQp−CaM complex and to determine the binding affinity of F-$Na_V1.2$ IQp for apo and calcium-saturated CaM. Fluorescence anisotropy measures the rate of tumbling of a fluorophore, which reflects the hydrodynamic radius of the molecule to which it is covalently connected. Large or extended molecules tumble at a slower rate and have larger anisotropy than molecules with a smaller hydrodynamic radius.

We found that the anisotropy of F-$Na_V1.2$ IQp increased as the peptide was titrated with either apo or calcium-saturated CaM_{1-148} (Figure 4A) or with either apo or calcium-saturated CaM_{76-148} (Figure 4B) and that the affinity of binding was high (dissociation constant in the nanomolar range). The insets in panels A and B of Figure 4 illustrate a 1:1 CaM:F-$Na_V1.2$ IQp stoichiometry. Attempts to fit the data to a one-site binding isotherm accounting for variations in end points and dilution of F-$Na_V1.2$ IQp (eq 5) indicated that the dissociation constant (K_d) for the interaction with CaM_{1-148} was ≤10 nM and that for the interaction with CaM_{76-148} was ≤25 nM (see Table 1). Simulations of eq 3 using 1 μM F-$Na_V1.2$ IQp and varying the K_d from 1 pM to 25 nM yielded nearly identical binding isotherms, consistent with these being stoichiometric conditions. It was not possible to infer whether there was a calcium-dependent difference in the affinity of F-$Na_V1.2$ IQp for CaM_{1-148} or CaM_{76-148}.

The association between F-$Na_V1.2$ IQp and CaM_{1-80} was much weaker than that for CaM_{1-148} or CaM_{76-148} (Figure 4C), with the greatest difference observed for apo CaM_{1-80} (see Figure 4C, dashed line). A complete titration of apo F-$Na_V1.2$ IQp with CaM_{1-80} was not experimentally achievable. However, these data were normalized to a maximum anisotropy assumed to be equal to that obtained upon saturation of the apo F-$Na_V1.2$ IQp−CaM_{1-80} solution with calcium. The normalized increase in the anisotropy of F-$Na_V1.2$ IQp upon titration with CaM_{1-80} was fit to a one-site binding isotherm (eq 3) with the two independent variables, $[CaM_{total}]$ and $[F\text{-}Na_V1.2\ IQp_{total}]$. The results listed in Table 1 indicate that the K_d for calcium-saturated CaM_{1-80} binding to F-$Na_V1.2$ IQp was reduced by a factor of ~25, from 132 ± 3 μM for apo CaM_{1-80} to 5.40 ± 2.96 μM for calcium-saturated CaM_{1-80} (Table 1).

Equilibrium Calcium Titrations of CaM in the Presence of $Na_V1.2$ IQp. To explore the effect of $Na_V1.2$ IQp on the calcium binding affinity of CaM, equilibrium calcium titrations of CaM_{1-148} in the presence of increasing molar ratios of $Na_V1.2$ IQp were monitored by measuring changes in the intrinsic fluorescence properties of CaM. The decrease in phenylalanine fluorescence upon calcium binding to sites I and II of CaM_{1-148} in the absence of $Na_V1.2$ IQp shown in Figure 5A (solid line) was fit to a model-independent two-site (Adair) function, accounting for variations in end points (eq 8) for resolving a total free energy of calcium binding to the N-domain of CaM_{1-148} of −13.01 ± 0.09 kcal/mol (Table 2).

Addition of an excess of $Na_V1.2$ IQp (from 1.4 to 1 CaM) enhanced the calcium binding affinity of the N-domain of CaM_{1-148} to −13.76 ± 0.16 kcal/mol. This 0.4-fold molar excess of $Na_V1.2$ IQp was determined to be saturating by subsequent experiments performed with 2.8-fold (Figure 5) and 4.0-fold molar excesses of $Na_V1.2$ IQp (*31*). The 0.75 ± 0.18 kcal/mol increase in ΔG_2 for the N-domain of CaM_{1-148} in the presence of $Na_V1.2$ IQp compared to that in the absence of $Na_V1.2$ IQp was small, but significant because it was larger than the standard deviation of at least three replicates and larger than the confidence intervals of individual analyses of each titration, which ranged from 0.04 to 0.05 kcal/mol.

Increases in the tyrosine fluorescence intensity were used to monitor calcium binding to sites III and IV in the

C-domain of CaM_{1-148} (Figure 5B). Stoichiometric calcium titrations of CaM in the presence of a molar excess of $Na_V1.2$ IQp showed that the signal from tyrosine residues within $Na_V1.2$ IQp (Y1916 and Y1919) did not contribute to the calcium-dependent tyrosine change measured for equilibrium calcium titrations with CaM and $Na_V1.2$ IQp mixtures (*31*). The increase in tyrosine fluorescence could thus be assigned to CaM. The calcium-dependent increase in tyrosine fluorescence was fit to eq 8, and the total free energy of calcium binding (ΔG_2) to sites III and IV in the C-domain of CaM_{1-148} was resolved to be -14.95 ± 0.14 kcal/mol in the absence of $Na_V1.2$ IQp and -12.89 ± 0.07 kcal/mol in the presence of a slight molar excess of $Na_V1.2$ IQp [1.4 to 1 CaM (Table 2)] that was determined to be saturating by subsequent studies performed with a 4-fold molar excess of $Na_V1.2$ IQp (*31*). This significant decrease of 2.06 ± 0.16 kcal/mol was larger than the standard deviation of at least three replicates and larger than the confidence intervals of individual analyses of each titration, which ranged from 0.01 to 0.04 kcal/mol.

Equilibrium calcium titrations of CaM_{1-80} (Figure 6A) and CaM_{76-148} (Figure 6B) in the absence and presence of $Na_V1.2$ IQp were used to probe the effect of $Na_V1.2$ IQp on the calcium binding affinity of each of the CaM domains. The resolved total free energy of calcium binding to sites I and II in CaM_{1-80} in the absence of $Na_V1.2$ IQp [$\Delta G_2 = -12.91 \pm 0.09$ kcal/mol (Table 2)] was very close to that measured for sites I and II in CaM_{1-148} [$\Delta G_2 = -13.01 \pm 0.09$ kcal/mol (Table 2)]. The addition of a 0.4-fold molar excess of $Na_V1.2$ IQp increased the ΔG_2 for calcium binding to CaM_{1-80} by 0.39 ± 0.09 kcal/mol to -13.30 ± 0.03 kcal/mol (Table 2). This increase was smaller than the 0.75 ± 0.18 kcal/mol increase observed for the N-domain of CaM_{1-148} but was significant because it was larger than the standard deviation of at least three replicates and larger than the confidence intervals of individual analyses of each titration, which ranged from 0.04 to 0.08 kcal/mol.

The resolved total free energy of calcium binding to sites III and IV in CaM_{76-148} in the absence of $Na_V1.2$ IQp [-14.81 ± 0.10 kcal/mol (Table 2)] was similar to that measured for sites III and IV in CaM_{1-148} [$\Delta G_2 = -14.95 \pm 0.14$ kcal/mol (Table 2)]. The addition of a 0.4-fold molar excess of $Na_V1.2$ IQp decreased the free energy for calcium binding to CaM_{76-148} by 2.12 ± 0.13 kcal/mol to -12.69 ± 0.08 kcal/mol. This decrease was identical to the 2.06 ± 0.16 kcal/mol decrease observed for the same sites in CaM_{1-148} and was larger than both the standard deviation of at least three replicates and the confidence intervals of individual analyses of each titration, the latter ranging from 0.02 to 0.04 kcal/mol.

Together, these data show that $Na_V1.2$ IQp reduced the calcium binding affinity of the C-domain of CaM to a value that was lower than the calcium binding affinity of the N-domain, thus reversing the hierarchy of calcium binding and reducing the energy difference between the domains as shown in Figure 8.

DISCUSSION

Domain-Specific Binding of CaM to the IQ Motif. To investigate the domain-specific association of CaM with $Na_V1.2$ IQp, changes in the secondary structure of apo and calcium-saturated CaM_{1-148}, CaM_{76-148}, and CaM_{1-80} upon addition of $Na_V1.2$ IQp were compared, as was the change in fluorescein emission of apo and calcium-saturated F-$Na_V1.2$ IQp upon addition of CaM_{1-148}, CaM_{76-148}, or CaM_{1-80}. The results consistently show that while the N-domain of calcium-saturated CaM can associate with $Na_V1.2$ IQp, the C-domain of CaM is necessary and sufficient for binding $Na_V1.2$ IQp, and this association is calcium-independent. These data suggest that CaM may be anchored to the C-terminal tail of $Na_V1.2$ via its C-domain during all stages of neuronal signaling (i.e., at all calcium concentrations). This model of CaM−ion channel interactions has been supported previously by data for calcium channels (*20*), NMDA receptors (*16*), and calcium-dependent potassium channels (*17*, *64*). Indeed, prelocalization of CaM to ion channels allows for a rapid CaM response to calcium, because it does not need to diffuse to the target channel but is already associated and primed to modulate the target as calcium levels change.

Effects of $Na_V1.2$ IQp on Calcium Binding. Most of the CaM-binding target proteins increase the calcium affinity of one or both CaM domains (*16*, *36*, *45*, *46*, *48*, *50*) or, in the case of neuromodulin, cause the release of CaM upon binding calcium (*45*). Increases in calcium binding affinity are thought to be the result of the target proteins covering exposed hydrophobic patches of CaM, which are created with the shift to the conformation required for calcium binding. Thus, the presence of a target lowers the free energy penalty associated with opening of the EF-hand domain, thereby facilitating formation of a more favorable metal-binding geometry for the 12 residues that comprise each calcium-binding site.

The interaction between CaM and $Na_V1.2$ IQp is particularly interesting in that $Na_V1.2$ IQp decreases the calcium affinity of the C-domain [$\Delta\Delta G_2 \sim 2.1$ kcal/mol (Table 2)] such that the two domains of CaM bind calcium with similar affinities. Association between CaM and the IQ-containing peptide representing the CaM-binding domain of neuromodulin showed a similar effect on the calcium binding affinity of CaM, where the affinity of the C-domain decreased by ~3-fold and the affinity of the N-domain increased by ~3-fold (*65*). The high-affinity interaction between $Na_V1.2$ IQp and the apo C-domain of CaM could potentially inhibit the transition to the open conformation required for calcium binding. This is suggested by the structure of apo CaM bound to IQ motifs 1 and 2 of the myosin V heavy chain; the C-domain of CaM is in a semi-open conformation, and the terminal Glu residues in calcium-binding sites III and IV are not correctly positioned for chelation (*42*).

In addition, calcium binding to the N-domain could potentially interrupt interdomain interactions. We found that in the context of CaM_{1-148} binding to $Na_V1.2$ IQp, the N-domain did not affect the calcium binding affinity of the C-domain (Table 2). The change in total free energy ($\Delta\Delta G_2$) for sites III and IV of CaM_{1-148} (with the N-domain) was 2.06 ± 0.16 kcal/mol versus 2.12 ± 0.13 kcal/mol for CaM_{76-148} (without the N-domain). The C-domain, however, did affect the calcium binding affinity of the N-domain slightly (Table 2) such that $\Delta\Delta G_2$ for sites I and II was -0.75 ± 0.18 kcal/mol for CaM_{1-148} (with the C-domain) versus -0.39 ± 0.09 kcal/mol for CaM_{1-80} (without the C-domain).

The C-domain thus exerts an influence over calcium binding to the N-domain, by ~0.36 kcal/mol, whereas the N-domain does not affect the calcium binding affinity of the C-domain within the levels of detection of these studies.

Linkage between Peptide and Calcium Binding to CaM. A simplified linkage diagram is proposed to summarize the effects of calcium and peptide binding with respect to the CaM−$Na_V1.2$ IQp interaction (Figure 7). In this model, calcium binding to CaM is represented along the horizontal axis, while $Na_V1.2$ IQp binding to CaM is represented along the vertical axis. According to the principle of conservation of free energy, the sum of ΔG_a and ΔG_b is equal to the sum of ΔG_c and ΔG_d (Figure 7). The linkage diagram demonstrates quantitatively that the decrease in calcium affinity of CaM originates from binding to $Na_V1.2$ IQp.

As stated above, $Na_V1.2$ IQp reduced the calcium binding affinity of both CaM_{1-148} and CaM_{76-148} by ~2.1 kcal/mol (Table 2). Anisotropy studies established that, under the experimental conditions used during equilibrium calcium titrations, CaM_{1-148} and CaM_{76-148} were saturated with $Na_V1.2$ IQp during the entire course of the experiment. It can be inferred from the linkage diagram that the 2.1 kcal/mol reduction in the calcium binding affinity of CaM sites III and IV that is due to the presence of $Na_V1.2$ IQp will result in the free energy of $Na_V1.2$ IQp binding to apo CaM (less than or equal to −12.9 kcal/mol) being 2.1 kcal/mol more favorable than binding to calcium-saturated CaM (less than or equal to −10.8 kcal/mol; $\Delta G_d > \Delta G_b$).

From anisotropy studies of F-$Na_V1.2$ IQp titrated with apo CaM_{1-80}, it can be estimated that at 3 μM CaM_{1-80} (concentration of CaM_{1-80} during equilibrium calcium titration) only ~2% of apo CaM_{1-80} is bound to $Na_V1.2$ IQp. This suggests that the calcium binding affinity determined for CaM_{1-80} in the presence of $Na_V1.2$ IQp did not represent that of CaM_{1-80} fully saturated with $Na_V1.2$ IQp. The resolved free energy of binding of apo CaM_{1-80} to $Na_V1.2$ IQp was −5.24 ± 0.02 kcal/mol (Table 1) and was approximately 2 kcal/mol less favorable than the free energy of binding of calcium-saturated CaM_{1-80} to $Na_V1.2$ IQp [−7.18 ± 0.35 kcal/mol (Table 1)]. On the basis of the thermodynamic cycle (Figure 7), one could extrapolate that if apo CaM_{1-80} were completely saturated by $Na_V1.2$ IQp and then titrated with calcium, an increase of ~2 kcal/mol (to −14.91 kcal/mol rather than −12.91 kcal/mol) would be measured as the total free energy of calcium binding to sites I and II. However, it is not technically feasible to conduct the experiment at sufficiently high CaM and $Na_V1.2$ IQp concentrations to test this prediction.

Fractional Population of Calcium Ligation States and Relation to Signaling. This study provides the first direct demonstration that the association of $Na_V1.2$ IQp with CaM causes a selective decrease in the calcium affinity of a single CaM domain such that the overall affinity of the protein is significantly reduced and the affinities of the two domains become similar with the N-domain now having a slightly higher affinity than the C-domain (Figures 5, 6, and 8A,C). This was independent of a covalent linkage of the N- and C-domains. The consequence of this interaction is reflected in the shift in the population of calcium-ligated species of CaM. The fractional populations of the calcium ligation states for CaM alone (Figure 8B) and for CaM bound by $Na_V1.2$ IQp (Figure 8D), based on the free energies reported in Table 2, illustrate that in the absence of $Na_V1.2$ IQp (panels A and B), the species whose CaM C-domains are saturated (0011) is populated much more extensively (62%) than the species whose N-domain is calcium-saturated (1100, barely observed at 2%). The maximum fraction of species 0011 is generated at a lower calcium concentration (3.8 μM) than the maximum fraction of species 1100 (5.7 μM) (Figure 8).

$Na_V1.2$ IQp significantly changes the fractional population of the calcium ligation states, as both CaM domains are maximally populated at nearly identical calcium concentrations (8.5 μM). However, the calcium-saturated N-domain (1100) populates much more extensively in the presence of $Na_V1.2$ IQp [28% (Figure 8D)], whereas the maximum population of the calcium-saturated C-domain (0011) is significantly reduced under these conditions [10% (Figure 8D)]. The maximal population of calcium-saturated N-domain increases by 1400% in the presence of $Na_V1.2$ IQp, whereas that for the calcium-saturated C-domain is reduced by 85% in the presence of $Na_V1.2$ IQp. This study illustrates a mechanism by which $Na_V1.2$ has fine-tuned the calcium affinity of CaM to respond in higher local calcium concentrations, allowing it to propagate inactivation signals to the $Na_V1.2$ C-terminal tail.

Comparison of VDSC Isoforms. Despite the high degree of sequence identity among the IQ-containing CaM-binding regions of all 10 known isoforms of the VDSC (*31*, *32*), there are significant differences in their effect on the thermodynamics of association with calmodulin. For example, the affinity of apo CaM for $Na_V1.2$ IQp ($K_d \leq 10$ nM) is at least 1000-fold more favorable than that for $Na_V1.5$ ($K_d = 0.16 \pm 0.04$ μM) (*43*). It will be exciting to compare the effect of these isoforms on the calcium binding affinity of CaM and how that translates into the role of CaM in channel inactivation.

Association of apo CaM with the C-terminal tail of the $Na_V1.6$ isoform increases the rate of VDSC inactivation, and high calcium concentrations reverse this effect (*29*). Both $Na_V1.2$ and $Na_V1.6$ isoforms are expressed in the central nervous system; however, $Na_V1.2$ is localized along unmyelinated sections of an axon, and $Na_V1.6$ is localized to the nodes of Ranvier in myelinated axons (*23*). Interestingly, $Na_V1.2$ is not as efficient at propagating action potentials as $Na_V1.6$. Our studies indicate that the cause of this reduced efficiency may be that $Na_V1.2$ lowers the calcium binding affinity of CaM, thereby requiring a higher calcium concentration to trigger a CaM-dependent response. The higher affinity of the N-domain compared to that of the C-domain of CaM when bound to $Na_V1.2$ IQp suggests that the N-domain may play a greater role in propagating action potentials of these channels than it does for other channels where the C-domain remains the higher-calcium affinity domain.

REFERENCES

1. Sorensen, B. R., Faga, L. A., Hultman, R., and Shea, M. A. (2002) Interdomain linker increases thermostability and decreases calcium affinity of calmodulin N-domain, *Biochemistry 41*, 15−20.
2. Faga, L. A., Sorensen, B. R., VanScyoc, W. S., and Shea, M. A. (2003) Basic Interdomain Boundary Residues in Calmodulin Decrease Calcium Affinity of Sites I and II by Stabilizing Helix-Helix Interactions, *Proteins: Struct., Funct., Genet. 50*, 381−391.

3. Crouch, T. H., and Klee, C. B. (1980) Positive Cooperative Binding of Calcium to Bovine Brain Calmodulin, *Biochemistry 19*, 3692−3698.
4. Wang, C.-L. A. (1985) A Note on Ca^{2+} Binding to Calmodulin, *Biochem. Biophys. Res. Commun. 130*, 426−430.
5. Pedigo, S., and Shea, M. A. (1995) Discontinuous Equilibrium Titrations of Cooperative Calcium Binding to Calmodulin Monitored by 1-D ^{1}H-Nuclear Magnetic Resonance Spectroscopy, *Biochemistry 34*, 10676−10689.
6. Linse, S., Helmersson, A., and Forsén, S. (1991) Calcium Binding to Calmodulin and Its Globular Domains, *J. Biol. Chem. 266*, 8050−8054.
7. Saimi, Y., and Kung, C. (2002) Calmodulin as an Ion-Channel Subunit, *Annu. Rev. Physiol. 64*, 289−311.
8. Crivici, A., and Ikura, M. (1995) Molecular and Structural Basis of Target Recognition by Calmodulin, *Annu. Rev. Biophys. Biomol. Struct. 24*, 85−116.
9. Yuan, T., Vogel, H. J., Sutherland, C., and Walsh, M. P. (1998) Characterization of the Ca^{2+}-dependent and -independent interactions between calmodulin and its binding domain of inducible nitric oxide synthase, *FEBS Lett. 431*, 210−214.
10. Yap, K. L., Kim, J., Truong, K., Sherman, M., Yuan, T., and Ikura, M. (2000) Calmodulin Target Database, *J. Struct. Funct. Genomics 1*, 8−14.
11. Vetter, S. W., and Leclerc, E. (2003) Novel aspects of calmodulin target recognition and activation, *Eur. J. Biochem. 270*, 404−414.
12. Chin, D., and Means, A. R. (2000) Calmodulin: A prototypical calcium sensor, *Trends Cell Biol. 10*, 322−328.
13. Hoeflich, K. P., and Ikura, M. (2002) Calmodulin in Action: Diversity in Target Recognition and Activation Mechanisms, *Cell 108*, 739−742.
14. Ehlers, M. D., Zhang, S., Bernhardt, J. P., and Huganir, R. L. (1996) Inactivation of NMDA receptors by direct interaction of calmodulin with the NR1 subunit, *Cell 84*, 745−755.
15. Zhang, S., Ehlers, M. D., Bernhardt, J. P., Su, C. T., and Huganir, R. L. (1998) Calmodulin mediates calcium-dependent inactivation of N-methyl-D-aspartate receptors, *Neuron 21*, 443−453.
16. Akyol, Z., Bartos, J. A., Merrill, M. A., Faga, L. A., Jaren, O. R., Shea, M. A., and Hell, J. W. (2004) Apo-Calmodulin Binds with its COOH-terminal Domain to the N-methyl-D-aspartate Receptor NR1 C0 Region, *J. Biol. Chem. 279*, 2166−2175.
17. Xia, X. M., Fakler, B., Rivard, A., Wayman, G., Johnson-Pais, T., Keen, J. E., Ishii, T., Hirschberg, B., Bond, C. T., Lutsenko, S., Maylie, J., and Adelman, J. (1998) Mechanism of calcium gating in small-conductance calcium-activated potassium channels, *Nature 395*, 503−507.
18. Peterson, B. Z., DeMaria, C. D., and Yue, D. T. (1999) Calmodulin Is the Ca^{2+} Sensor for Ca^{2+}-Dependent Inactivation of L-Type Calcium Channels, *Neuron 22*, 549−558.
19. Qin, N., Olcese, R., Bransby, M., Lin, T., and Birnbaumer, L. (1999) Ca^{2+}-induced inhibition of the cardiac Ca^{2+} channel depends on calmodulin, *Proc. Natl. Acad. Sci. U.S.A. 96*, 2435−2438.
20. Lee, A., Wong, S. T., Gallagher, D., Li, B., Storm, D. R., Scheuer, T., and Catterall, W. A. (1999) Ca^{2+}/calmodulin binds to and modulates P/Q-type calcium channels, *Nature 399*, 155−159.
21. Mori, M., Konno, T., Ozawa, T., Murata, M., Imoto, K., and Nagayama, K. (2000) Novel Interaction of the Voltage-Dependent Sodium Channel (VDSC) with Calmodulin: Does VDSC Acquire Calmodulin-Mediated Ca^{2+}-Sensitivity? *Biochemistry 39*, 1316−1323.
22. Trimmer, J. S., and Rhodes, K. J. (2004) Localization of Voltage-Gated Ion Channels in Mammalian Brian, *Annu. Rev. Phys. 66*, 477−519.
23. Schaller, K. L., and Caldwell, J. H. (2003) Expression and distribution of voltage-gated sodium channels in the cerebellum, *Cerebellum 2*, 2−9.
24. Catterall, W. A. (2000) From Ionic Currents to Molecular Mechanisms: The Structure and Function of Voltage-Gated Sodium Channels, *Neuron 26*, 13−25.
25. Yu, F. H., and Catterall, W. A. (2003) Overview of the voltage-gated sodium channel family, *GenomeBiology 4*, 207.1−207.7.
26. Mantegazza, M., Yu, F. H., Catterall, W. A., and Scheuer, T. (2001) Role of the C-terminal domain in inactivation of brain and cardiac sodium channel, *Proc. Natl. Acad. Sci. U.S.A. 98*, 15348−15353.
27. Deschênes, I., Trottier, E., and Chahine, M. (2001) Implication of the C-Terminal Region of the α-Subunit of Voltage-gated Sodium Channels in Fast Inactivation, *J. Membr. Biol. 183*, 103−114.
28. Cormier, J. W., Rivolta, I., Tateyama, M., Yang, A. S., and Kass, R. S. (2002) Secondary Structure of the Human Cardiac Na^+ Channel C Terminus, *J. Biol. Chem. 277*, 9233−9241.
29. Herzog, R. I., Liu, C., Waxman, S. G., and Cummins, T. R. (2003) Calmodulin Binds to the C Terminus of Sodium Channels $Na_v1.4$ and $Na_v1.6$ and Differentially Modulates Their Functional Properties, *J. Neurosci. 23*, 8261−8270.
30. Bähler, M., and Rhoads, A. (2002) Calmodulin signaling via the IQ motif, *FEBS Lett. 513*, 107−113.
31. Theoharis, N. T. (2004) Neuronal voltage-dependent sodium channel type II selectively decreases the calcium-binding affinity of the C-domain of Calmodulin, M.S. Dissertation. University of Iowa, Iowa City, IA.
32. Chenna, R., Sugawara, H., Koike, T., Lopez, R., Gibson, T. J., Higgins, D. G., and Thompson, J. D. (2003) Multiple sequence alignment with the Clustal series of programs, *Nucleic Acids Res. 31*, 3497−500.
33. Deschênes, I., Neyroud, N., DiSilvestre, D., Marbán, E., Yue, D. T., and Tomaselli, G. F. (2002) Isoform-Specific Modulation of Voltage-Gated Na^+ Channels by Calmodulin, *Circ. Res. 90*, E49−E57.
34. Tan, H. L., Kupershmidt, S., Zhang, R., Stepanovic, S., Roden, D. M., Wilde, A. A. M., Anderson, M. E., and Balser, J. R. (2002) A calcium sensor in the sodium channel modulates cardiac excitability, *Nature 415*, 442−447.
35. Kung, C., Preston, R. R., Maley, M. E., Ling, K.-Y., Kanabrocki, J. A., Seavey, B. R., and Saimi, Y. (1992) *In vivo Paramecium* mutants show that calmodulin orchestrates membrane responses to stimuli, *Cell Calcium 13*, 413−425.
36. Xiong, L. W., Newman, R. A., Rodney, G. G., Thomas, O., Zhang, J. Z., Persechini, A., Shea, M. A., and Hamilton, S. L. (2002) Lobe-dependent regulation of ryanodine receptor type 1 by calmodulin, *J. Biol. Chem. 277*, 40862−40870.
37. Liang, H., DeMaria, C. D., Erickson, M. G., Mori, M. X., Alseikhan, B. A., and Yue, D. T. (2003) Unified mechanisms of Ca^{2+} regulation across the Ca^{2+} channel family, *Neuron 39*, 951−960.
38. van Petegem, F., Chatelain, F. C., and Minor, D. L., Jr. (2005) Insights into voltage-gated calcium channel regulation from the structure of the $Ca_{(V)}1.2$ IQ domain-Ca^{2+}/calmodulin complex, *Nat. Struct. Mol. Biol. 12*, 1108−1115.
39. Ikura, M., Clore, G. M., Gronenborn, A. M., Zhu, G., Klee, C. B., and Bax, A. (1992) Solution structure of a calmodulin-target peptide complex by multidimensional NMR, *Science 256*, 632−638.
40. Drum, C. L., Yan, S., Bard, J., Shen, Y., Lu, D., Soelaiman, S., Grabarek, Z., Bohm, A., and Tang, W. (2002) Structural basis for the activation of anthrax adenylyl cyclase exotoxin by calmodulin, *Nature 415*, 396−402.
41. Schumacher, M. A., Rivard, A. F., Bachinger, H. P., and Adelman, J. P. (2001) Structure of the gating domain of a Ca^{2+}-activated K^+ channel complexed with Ca^{2+}/calmodulin, *Nature 410*, 1120−1124.
42. Houdusse, A., Gaucher, J. F., Krementsova, E., Mui, S., Trybus, K. M., and Cohen, C. (2006) Crystal structure of apo-calmodulin bound to the first two IQ motifs of myosin V reveals essential recognition features, *Proc. Natl. Acad. Sci. U.S.A. 103*, 19326−31.
43. Shah, V. N., Wingo, T. L., Weiss, K. L., Williams, C. K., Balser, J. R., and Chazin, W. J. (2006) Calcium-dependent regulation of the voltage-gated sodium channel hH1: Intrinsic and extrinsic sensors use a common molecular switch, *Proc. Natl. Acad. Sci. U.S.A. 103*, 3592−3597.
44. Kim, J., Ghosh, S., Liu, H., Tateyama, M., Kass, R. S., and Pitt, G. S. (2004) Calmodulin mediates Ca^{2+} sensitivity of sodium channels, *J. Biol. Chem. 279*, 45004−45012.
45. Jurado, L. A., Chockalingam, P. S., and Jarrett, H. W. (1999) Apocalmodulin, *Physiol. Rev. 79*, 661−682.
46. Peersen, O. B., Madsen, T. S., and Falke, J. J. (1997) Intermolecular tuning of calmodulin by target peptides and proteins: Differential effects on Ca^{2+} binding and implications for kinase activation, *Protein Sci. 6*, 794−807.

47. Bayley, P. M., Findlay, W. A., and Martin, S. R. (1996) Target recognition by calmodulin: Dissecting the kinetics and affinity of interaction using short peptide sequences, *Protein Sci. 5*, 1215−1228.
48. Johnson, J. D., Snyder, C., Walsh, M., and Flynn, M. (1996) Effects of myosin light chain kinase and peptides on Ca^{2+} exchange with the N- and C-terminal Ca^{2+} binding sites of calmodulin, *J. Biol. Chem. 271*, 761−767.
49. Martin, S. R., Bayley, P. M., Brown, S. E., Porumb, T., Zhang, M., and Ikura, M. (1996) Spectroscopic characterization of a high-affinity calmodulin-target peptide hybrid molecule, *Biochemistry 35*, 3508−3517.
50. Tang, W., Halling, D. B., Black, D. J., Pate, P., Zhang, J. Z., Pedersen, S., Altschuld, R. A., and Hamilton, S. L. (2003) Apocalmodulin and Ca^{2+} Calmodulin-Binding Sites on the $Ca_V1.2$ Channel, *Biophys. J. 85*, 1538−1547.
51. Sorensen, B. R., and Shea, M. A. (1998) Interactions between domains of apo calmodulin alter calcium binding and stability, *Biochemistry 37*, 4244−4253.
52. Putkey, J. A., Slaughter, G. R., and Means, A. R. (1985) Bacterial expression and characterization of proteins derived from the chicken calmodulin cDNA and a calmodulin processed gene, *J. Biol. Chem. 260*, 4704−4712.
53. Beaven, G. H., and Holiday, E. R. (1952) Ultraviolet absorbtion spectra of proteins and amino acids, *Adv. Protein Chem. 7*, 319−386.
54. Lakowicz, J. R. (1999) *Principles of Fluorescence Spectroscopy*, Kluwer Academic/Plenum Publishing, New York.
55. Johnson, M. L., and Frasier, S. G. (1985) Nonlinear least-squares analysis, *Methods Enzymol. 117*, 301−342.
56. Klotz, I. M. (1986) Ligand-Receptor Interactions, in *Introduction to Biomolecular Energetics*, pp 103−133, Academic Press, Inc., Orlando, FL.
57. Winzor, D. J., and Sawyer, W. H. (1995) Spectral Studies of Ligand Binding, in *Quantitative Characterization of Ligand Binding*, pp 28−46, Wiley-Liss, Inc., New York.
58. VanScyoc, W. S., and Shea, M. A. (2001) Phenylalanine fluorescence studies of calcium binding to N-domain fragments of *Paramecium* calmodulin mutants show increased calcium affinity correlates with increased disorder, *Protein Sci. 10*, 1758−1768.
59. Pedigo, S., and Shea, M. A. (1995) Quantitative endoproteinase GluC footprinting of cooperative Ca^{2+} binding to calmodulin: Proteolytic susceptibility of E31 and E87 indicates interdomain interactions, *Biochemistry 34*, 1179−1196.
60. Shea, M. A., Sorensen, B. R., Pedigo, S., and Verhoeven, A. (2000) Proteolytic Footprinting Titrations for Estimating Ligand-Binding Constants and Detecting Pathways of Conformational Switching of Calmodulin, *Methods Enzymol. 323*, 254−301.
61. Jaren, O. R., Harmon, S., Chen, A. F., and Shea, M. A. (2000) *Paramecium* Calmodulin Mutants Defective in Ion Channel Regulation Can Bind Calcium and Undergo Calcium-Induced Conformational Switching, *Biochemistry 39*, 6881−6890.
62. Mori, M., Konno, T., Morii, T., Nagayama, K., and Imoto, K. (2003) Regulatory interaction of sodium channel IQ-motif with calmodulin C-terminal lobe, *Biochem. Biophys. Res. Commun. 307*, 290−296.
63. Tsalkova, T. N., and Privalov, P. L. (1985) Thermodynamic Study of Domain Organization in Troponin C and Calmodulin, *J. Mol. Biol. 181*, 533−544.
64. Keen, J. E., Khawaled, R., Farrens, D. L., Neelands, T., Rivard, A., Bond, C. T., Janowsky, A., Fakler, B., Adelman, J. P., and Maylie, J. (1999) Domains responsible for constitutive and Ca^{2+}-dependent interactions between calmodulin and small conductance Ca^{2+}-activated potassium channels, *J. Neurosci. 19*, 8830−8838.
65. Black, D. J., Leonard, J., and Persechini, A. (2006) Biphasic Ca^{2+}-dependent switching in a calmodulin-IQ domain complex, *Biochemistry 45*, 6987−6995.
66. Chattopadhyaya, R., Meador, W. E., Means, A. R., and Quiocho, F. A. (1992) Calmodulin Structure Refined at 1.7 Å Resolution, *J. Mol. Biol. 228* (4), 1177−1192.

BI7013129